In Situ Surface-Enhanced Raman Spectroscopic Studies of CO Adsorption and Methanol Oxidation on Ru-Modified Pt Surfaces

ARTICLE *in* THE JOURNAL OF PHYSICAL CHEMISTRY C · DECEMBER 2007

Impact Factor: 4.77 · DOI: 10.1021/jp075929l

3 AUTHORS, INCLUDING:

Hongzhou Yang
Miami University
26 PUBLICATIONS **1,019** CITATIONS

SEE PROFILE

Shouzhong Zou
American University Washington D.C.
74 PUBLICATIONS **2,437** CITATIONS

SEE PROFILE

In Situ Surface-Enhanced Raman Spectroscopic Studies of CO Adsorption and Methanol Oxidation on Ru-Modified Pt Surfaces

Hongzhou Yang, Yuqing Yang, and Shouzhong Zou*

Department of Chemistry and Biochemistry, Miami University, Oxford, Ohio 45056

Received: July 26, 2007; In Final Form: September 2, 2007

Ru-modified Pt is so far the best catalyst for the anode reaction of direct methanol fuel cells. The role of Ru is believed to promote carbon monoxide oxidation through a bifunctional mechanism and an electronic effect. However, direct experimental evidence for the electronic effect is sparse. In addition, whether Ru oxides or metallic Ru is the active component in the catalyst is still under debate. To address these issues, carbon monoxide adsorption and methanol oxidation on Ru-modified Pt thin film surfaces in acidic media were studied using in situ overlayer surface-enhanced Raman spectroscopy (SERS). Cyclic voltammograms show that with the presence of Ru, CO and methanol oxidation is significantly enhanced as evident by the negative shift of the oxidation potential. The addition of Ru to Pt surfaces did not change the Pt−CO stretching frequency, suggesting that the Pt−CO bond is not weakened significantly by Ru. Through combined SERS and cyclic voltammetry studies, we found that Pt and Ru oxides are inhibitors for methanol oxidation. In particular, Ru oxides on Ru-modified Pt strongly inhibit methanol oxidation on Pt sites, even when the Pt sites are in the metallic state.

Introduction

The PtRu catalyst is widely recognized as the best anode catalyst for the direct methanol fuel cell (DMFC).[1−4] Its high catalytic activity as compared to pure Pt is generally explained by a bifunctional mechanism.[5] In this mechanism, methanol oxidation occurs on Pt to form carbon monoxide (CO), which is a surface poison blocking further methanol oxidation, whereas the hydroxyl species that is the oxidant for CO removal is formed on the Ru sites at a potential about 200 mV more negative than on pure Pt, facilitating the overall reaction. An additional factor contributing to the activity improvement on PtRu is the so-called ligand effect or electronic effect.[6−9] It is suggested that the addition of Ru to Pt weakens the Pt−CO bond and therefore promotes the CO oxidation.[6−9]

Despite significant progress in understanding methanol oxidation on PtRu surfaces, several important issues are still under active debate. For the ligand effect, there are theoretical and experimental studies suggesting the weakening of the Pt−CO bond by Ru. Temperature-programmed desorption spectra of CO on Ru-modified Pt[10] and submonolayer Pt-covered Ru(0001)[7] surfaces carried out under ultrahigh vacuum (UHV) show that CO desorption occurs at a lower temperature as compared to the corresponding pure metals, indicative of a lower CO adsorption energy on the modified surfaces in this environment. A recent electrochemical NMR spectroscopic study also demonstrated the modification of Pt electronic structure by the addition of Ru.[9] In situ X-ray absorption spectroscopy shows that the addition of Ru shortens the Pt−Pt bond length and increases the Pt d band vacancy.[11] In situ FTIR and, more recently, vibration sum frequency generation (SFG) have been applied to study CO and methanol adsorption and oxidation on model PtRu catalysts.[12−19] The bands from the adsorbed CO (CO_{ads}) and the oxidation product CO_2 dissolved in the solutions contain rich information about the reaction mechanism. The C−O stretching frequency of CO_{ads} is sometimes used to infer the Pt−CO bond strength change.[20] This practice is, however, complicated by a vibrational dipole coupling effect, which is sensitive to the surface structure of PtRu catalysts.[21] Density functional theory calculations show a drastic red-shift (up to 60 cm^{-1}) of the Pt−CO stretching frequency.[22,23] However, in situ direct detection of Pt−CO bond weakening has not been reported.

Another issue concerns the chemical state of the ruthenium involved in the methanol oxidation. In the previous work, it was demonstrated that the practical PtRu black alloys are mixed phase materials composed of metallic Pt, hydrous Pt oxides, and hydrous as well as dehydrated RuO_2, and that only a minor fraction (<25%) of Ru is present as the metallic phase.[24,25] Some experimental results suggest that in the PtRu catalysts, Pt^0Ru^0 is less active for methanol oxidation than a mixed phase electrocatalyst containing Pt metal and hydrous ruthenium oxides.[26,27] Contrary results have also been observed for the role of ruthenium oxides. Lasch et al. claimed that the presence of an alloyed metallic Pt−Ru phase as well as the amorphous hydrated Ru oxides are favorable for methanol oxidation.[28] Kim et al. investigated the relationships between the oxidation states of ruthenium and the methanol oxidation activity on Ru-modified Pt(111) electrodes by X-ray photoelectron spectroscopy (XPS) and chronoamperometry.[29] They concluded that the ruthenium oxides acted as a catalytic de-enhancer rather than a promoter, and therefore, the presence of a Ru metallic phase is a prerequisite for effective methanol oxidation. In situ X-ray absorption spectroscopic studies also point out the importance of metallic Ru in the PtRu catalysts.[30−32]

In this work, we report results from our recent efforts in utilizing in situ overlayer surface-enhanced Raman spectroscopy (SERS) to address the above important issues. There have been ample examples demonstrating that SERS is a versatile and powerful technique for investigating both solid/liquid and

* To whom correspondence should be addressed. Tel.: (513) 529-8084; fax: (513) 529-5715; e-mail: zous@muohio.edu.

10.1021/jp075929l CCC: $37.00
Published on Web 12/05/2007

solid/gas interfaces.[33−35] Originally only applicable to coinage metals, recent developments have shown that SERS can also be applied to Pt group and other transition metals, either by depositing the metals as ultrathin films on a SERS-active Au substrate (the so-called overlayer SERS)[36,37] or by significantly roughening the metals themselves.[38,39] Its high surface sensitivity and ability to detect metal−adsorbate and metal oxide vibrations make SERS particularly suitable for tackling the problems stated above. Although the necessity to use roughened surfaces to obtain the Raman enhancement effect precludes its applicability to well-defined single-crystal surfaces, its capability of simultaneously probing the metal−adsorbate and intramolecular bonding should provide complimentary information to SFG and the much more extensively employed surface infrared spectroscopy. Surprisingly, there is only one previous report on the in situ SERS study of methanol oxidation on PtRu surfaces.[40] In our previous work, it was found that methanol oxidation does occur at room temperature on Ru surfaces at the potential where the methanol oxidation peak current is typically observed on PtRu catalysts.[41] Here, we show that the addition of Ru does not significantly weaken the Pt−CO bond on the Ru-modified Pt model catalysts. The combined SERS and cyclic voltammetry studies clearly demonstrate that ruthenium oxides inhibit methanol oxidation on Pt sites, even if the Pt sites are in the metallic state. These new insights should shed new light on the mechanisms of methanol oxidation on PtRu catalysts.

Experimental Procedures

Potassium tetrachloroplatinate (K_2PtCl_4), copper sulfate ($CuSO_4$), and ruthenium chloride ($RuCl_3$) were obtained from Sigma-Aldrich (St. Louis, MO). HPLC grade methanol was from Pharmco (Brookfield, CT), and carbon monoxide (99.995%) was from Linde Gas (Murray Hill, NJ). Double-distilled perchloric acid ($HClO_4$) and sulfuric acid (H_2SO_4) were from GFS chemicals (Powell, OH). The aqueous solutions were prepared using Milli-Q water from a Millipore water purification system (Milli-Q A10, Millipore, MA).

In a typical sample preparation, a Au electrode (2 mm in diameter, CH Instruments, Austin, TX) was polished with 1.0 and 0.3 μm Al_2O_3 powder successively on a polishing cloth (Buehler, Lake Bluff, IL) and then roughened by electrochemical oxidation−reduction cycles in a 0.1 M KCl aqueous solution to obtain a Raman enhancement effect as described by Gao et al.[42] Pt monolayer (ML) films were deposited by a redox replacement method.[36,43] First, the Cu underpotential deposition (UPD) was carried out on the roughened Au electrode in a 0.1 M H_2SO_4 and 1 mM $CuSO_4$ solution by holding the potential at 0.05 V versus Ag/AgCl for 2 min. Then, the Au electrode coated with the Cu UPD layer was immersed in a solution containing 5 mM K_2PtCl_4 and 0.1 M $HClO_4$ for 4 min to ensure the complete replacement of Cu with Pt. This process was repeated one more time to form nominally 2 ML of Pt on the Au electrode surface. The ruthenium deposition on 2 ML Pt-covered Au electrodes was typically carried out by constant potential deposition in 5 mM $RuCl_3$ and 0.1 M $HClO_4$.[44] Before ruthenium deposition, the $RuCl_3$ solution was aged for 2 weeks to obtain a stable brown solution and reproducible deposition results. By varying deposition time and potential, different ruthenium coverages can be obtained. Because the cyclic voltammogram obtained from the ruthenium film on the roughened Au electrode in 0.1 M $HClO_4$ does not show a significant hydrogen adsorption−desorption current (Figure S1), ruthenium coverage on the Pt film surface was calculated from the difference of the hydrogen adsorption/desorption charge at the Pt surface before and after the Ru deposition. The hydrogen charge was obtained from the cyclic voltammogram of the electrode in 0.1 M $HClO_4$ with a 100 mV/s scan rate and between −0.25 and +0.8 V. For the combined Raman and cyclic voltammetry (CV) experiments or slow scan (1 mV/s) CV, the Ru coverage was accessed after the Raman or cyclic voltammogram acquisition. The Ru coverage after the experiment decreases due to the dissolution of RuO_2 at high potentials and the slow scan rate (1 mV/s), but the change is smaller than 0.04. Such a small change will not affect the overall interpretation of the results. In the present work, Ru decorated Pt film electrodes obtained by this method are denoted as 2 ML Pt/Ru-*x*, where *x* is the ruthenium coverage on the Pt surface. The ruthenium deposition on the roughened Au electrode was carried out by constant potential deposition in 5 mM $RuCl_3$ and 0.1 M $HClO_4$ as described by Wilke et al.[45]

Cyclic voltammograms were recorded with an electrochemical analyzer (CHI 630 A, CH Instruments, Austin, TX). Surface-enhanced Raman measurements were performed in a two-compartment, three-electrode glass cell with an optically flat glass disc as the window at the bottom. A Pt wire was used as the counter electrode, and a Ag/AgCl electrode with a saturated KCl aqueous solution was the reference electrode. For potential step experiments, the electrode potential was controlled by a voltammograph (CV27, BAS, West Lafayette, IN). Raman spectra were collected with a portable micro-Raman probe system as described elsewhere.[46,47] Briefly, a laser excitation at 785 nm from a diode laser was focused to a 100 μm spot on the sample with a long working distance 20× microscope objective (NA 0.42). The Raman scattering light was collected with the same objective in a back-scattering fashion and sent to a monochromator. The laser power on the sample was typically 20 mW. The Raman shift axis was calibrated with neon light. A typical spectrum acquisition time was either 20 or 60 s unless otherwise noted. The spectra were plotted with the intensity converted to electron counts per second (cps) and were subjected to a multi-point baseline correction using GRAMS AI program (Thermo Galactic, Salem, NH). All of the measurements were conducted at room temperature (22 ± 1 °C).

Results and Discussion

CV. Of central interest in this work is the examination of the effects of Ru on the CO adsorption and methanol oxidation at Pt surfaces by in situ surface-enhanced Raman spectroscopy. To obtain strong SERS signals, Ru-modified Pt monolayers deposited on roughened Au electrodes were used. Previous works of CO and methanol oxidation on PtRu systems have been focused on Ru-modified Pt single-crystal surfaces,[48−50] PtRu alloys,[51] and Ru-modified Pt nanoparticles supported on carbon.[52] No information about the electrooxidation of CO and methanol on Ru-modified Pt monolayers is available. We therefore first examined the cyclic voltammograms of CO and methanol oxidation on these surfaces.

Figure 1 shows the cyclic voltammograms of CO and methanol (MeOH) oxidation on 2 ML Pt and Ru-modified 2 ML Pt surfaces. For CO oxidation, the irreversibly adsorbed CO layer was formed by exposing the electrode surface to CO-saturated 0.1 M $HClO_4$ for 5 min with the potential held at −0.2 V. The solution phase CO was then removed by purging N_2 for 10 min with the electrode potential controlled at the same value before the voltammogram was recorded. On 2 ML Pt, the CO oxidation began at around 0.4 V (Figure 1A), yielding a sharp oxidation peak at about 0.42 V. This observation is

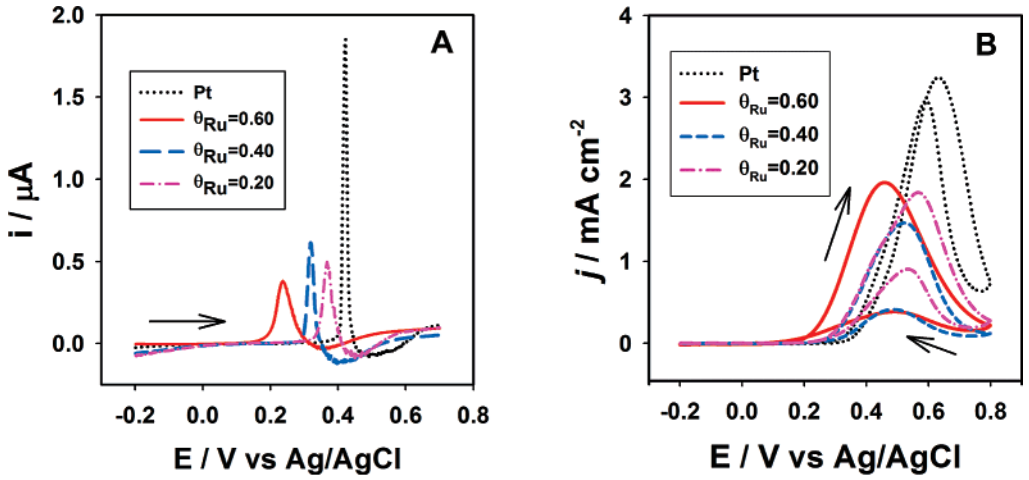

Figure 1. (A) CO stripping voltammograms obtained on CO-covered 2 ML Pt and Ru-modified 2 ML Pt films with various Ru coverages in 0.1 M $HClO_4$. (B) Cyclic voltammograms of 2 ML Pt and Ru-modified 2 ML Pt in 1 M MeOH + 0.1 M $HClO_4$. Scan rate: 1 mV s^{-1}. The arrows indicate the electrode potential scan direction.

similar to that seen on a bulk polycrystalline Pt electrode, suggesting that the two surfaces have similar CO oxidation activity. With the addition of Ru to the Pt surface, the CO oxidation potential shifted significantly to more negative values. With about 20% of the Pt surface covered by Ru, the CO oxidation peak position shifted from 0.42 to 0.37 V. Upon increasing the Ru coverage, the CO oxidation peak potential moved even more negatively, from 0.32 V at $\theta_{Ru} = 0.4$ to 0.24 V at $\theta_{Ru} = 0.6$. The negative shift of CO oxidation peak potential indicates an increasing CO oxidation activity on the Ru-modified Pt surfaces. The highest activity was obtained at $\theta_{Ru} = 0.6$, roughly in agreement with the results from PtRu alloy surfaces where the lowest CO oxidation peak potential was observed at $\theta_{Ru} = 0.5$.[53]

We now turn to methanol oxidation. For methanol oxidation on 2 ML Pt, a measured amount of methanol was introduced into 0.1 M $HClO_4$ to make up 1 M MeOH in the solution with the electrode potential being held at −0.2 V. A similar procedure was applied to the Ru-modified 2 ML Pt, except that prior to the methanol addition, the electrode was held at −0.4 V for 3 min to reduce ruthenium oxides inevitably formed during the transfer of the electrode in air from the Ru deposition cell. The removal of the oxides was signified by the disappearance of the characteristic Raman bands. The cyclic voltammograms were recorded between −0.2 and +0.8 V with the potential scan started at −0.2 V. The current density was calculated using the Pt area obtained from the average of hydrogen adsorption and desorption charges, assuming that the charge involved in the adsorption/desorption of 1 ML H_{ads} is 210 $\mu C/cm^2$.[54]

On a 2 ML Pt film, the methanol oxidation current took off at around 0.35 V and reached a peak value at 0.63 V. In the cathodic scan, the peak position shifted to 0.59 V. Upon addition of Ru to the Pt film, the methanol oxidation was significantly enhanced as evident by the negative shift of the onset and peak potentials (Figure 1B). The magnitude of the negative potential shift increased with the amount of Ru on the Pt film surface. When the Ru coverage reached 0.6, the methanol oxidation peak potential was at 0.46 V, 170 mV more negative than that on the pure Pt film. It has been shown that the composition for the highest activity of methanol oxidation on PtRu alloy surfaces is about 10−20% Ru. The demarcation from this value suggests that the Ru deposits form islands, as is confirmed by the spectroscopic data (vide infra). The Ru coverage for the maximal methanol oxidation activity on the Ru-modified Pt surfaces formed by spontaneous deposition was found to be between 0.2 and 0.6,[55,56] largely in agreement with the findings described here. In addition to the negative shift of the methanol oxidation potential, the presence of Ru on the Pt surfaces renders a much smaller methanol oxidation peak current on the cathodic scan. A similar observation was obtained on Ru-modified Pt(111) and explained in terms of the availability of Pt sites for methanol adsorption.[56] On the basis of the simultaneously recorded SER spectra, we argue that this decrease of methanol oxidation peak current is due to the formation of ruthenium oxides that inhibit the reaction (vide infra). Further support for this explanation can be found in the subsequent potential cycle, in which the methanol oxidation peak current was nearly identical to that of the first anodic scan. On all of the surfaces, the methanol oxidation current takes off at the potential where CO oxidation starts (Figure 1), suggesting that the methanol oxidation is indeed blocked by adsorbed CO. With the addition of Ru to Pt, the current density of methanol oxidation at the peak potential becomes smaller. This observation is different from that obtained on the Ru-modified Pt(111) surfaces, where a higher current density is typically seen.[56,57] We suspect that the different deposition procedure and the use of a polycrystalline Pt film in the present study may be responsible for this difference.

SERS of Adsorbed CO. To reveal the effects of Ru on the CO adsorption on Pt, we used SERS. As stated in the outset, SERS allows the direct detection of the metal−CO stretching band, which contains the information regarding the metal−CO bonding. Shown in Figure 2 is a set of SER spectra of irreversibly adsorbed CO on 2 ML Pt, Ru-modified 2 ML Pt with different Ru coverages, and pure Ru films acquired at −0.2 V in 0.1 M $HClO_4$. Each spectrum was acquired on a separately roughened Au electrode covered with the corresponding metal overlayers. The change of Raman intensity with different Ru coverage reflects the variation of SERS activity of Au electrodes. The CO adlayer was formed by first purging the gas into the solution for 5 min followed by N_2 sparging for 10−15 min to remove solution phase CO with the potential held at −0.2 V. To ensure accurate determination of the vibration band frequency, a 1200 groove/mm grating was used, which yields a spectral resolution of 2 cm^{-1} and a spectral range of 600−700 cm^{-1}. The lower frequency region spectrum showing the M−CO stretch (ν_{M-CO}) was obtained in tandem with the corresponding higher frequency partner containing C−O stretching (ν_{CO}) bands. Starting from the higher frequency region, on 2 ML Pt two ν_{CO} bands were observed (top spectrum, Figure 2B), and the weak feature at about 1865 cm^{-1} can be assigned to the bridge

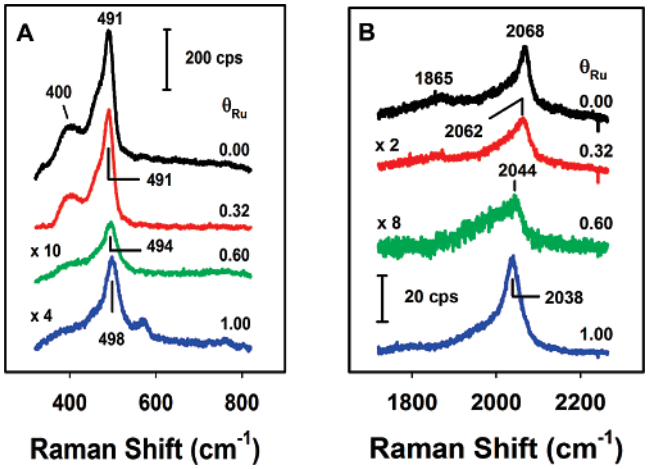

Figure 2. SER spectra obtained on 2 ML Pt, Ru-modified 2 ML Pt, and Ru in 0.1 M $HClO_4$ with CO irreversibly adsorbed on the surfaces. The spectra cover both metal−CO stretching (A) and C−O stretching (B) regions. Spectrograph grating: 1200 g/mm. The Ru coverage is indicated alongside the corresponding spectrum. The electrode potential is held at −0.2 V. $\theta_{Ru} = 1.00$ denotes the Ru film.

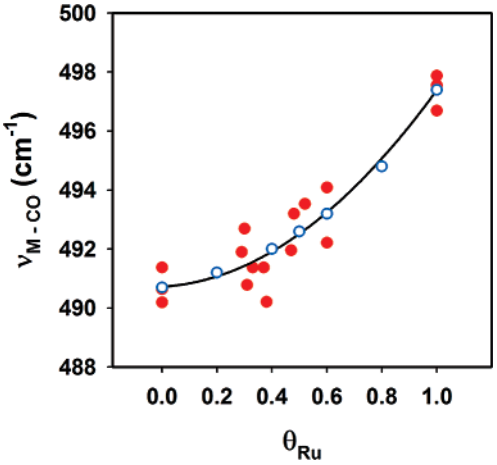

Figure 3. Metal−CO stretching frequency as a function of Ru coverage. Solid circles: experimental results and open circles: calculated values. The line serves only as a guide to the eyes.

adsorbed CO, while the much stronger band at 2068 cm^{-1} is from the atop adsorbed CO.[37,58] Upon addition of Ru to the Pt surface, the atop adsorbed ν_{CO} shifted to a lower frequency and reached around 2040 cm^{-1} on pure Ru. As the Ru coverage increased, the bridging CO band disappeared and was not discernible on the pure Ru film. The Ru coverage-dependent ν_{CO} shift agreed well with the in situ FTIR results from Ru-decorated Pt single-crystal and nanoparticle surfaces.[15,48,59] The strong tailing of the main atop CO band at the lower frequency side prohibits the observation of ν_{CO} from CO on Ru sites; therefore, it is difficult to tell as to whether there are two distinguishable ν_{CO} bands as have been observed in infrared spectra from the Ru-modified Pt single crystals and nanoparticles.[15,48,59]

Of particular interest in the present study is the direct probing of the Pt−CO bonding change as a function of Ru coverage. This information can be obtained from the metal−CO stretching frequency in the lower frequency region of the spectra. Although the shift of the ν_{CO} frequency is often used to infer the metal−CO bonding change, it provides only indirect information, and other factors such as vibration dipole−dipole coupling can contribute significantly to the ν_{CO} shift.[15,21] As shown in Figure 2A, a strong band at about 491 cm^{-1} can be attributed to Pt−CO stretching (ν_{Pt-CO}) from atop CO and a weaker peak at 400 cm^{-1} to ν_{Pt-CO} from bridging CO.[45,60] With the addition of Ru, the metal−CO stretching (ν_{M-CO}) band gradually shifted to higher values and finally approached the Ru−CO stretching (ν_{Ru-CO}) frequency at 498 cm^{-1}.

The proximity of ν_{Pt-CO} and ν_{Ru-CO} and the broadness of the bands preclude the observation of two separate M−CO bands. The blue-shift of the metal−CO stretching is further demonstrated by a ν_{M-CO} versus ruthenium coverage (θ_{Ru}) plot that includes additional data points with various θ_{Ru} values (Figure 3). The ν_{M-CO} value increases nearly linearly with θ_{Ru}, skewed toward the ν_{Pt-CO} value. This frequency bias arises from the fact that Ru is deposited on top of the Pt film, rendering a lower intensity of ν_{Ru-CO} than that of ν_{Pt-CO} on the Ru-modified Pt because the SERS intensity decays rapidly with the distance from the Au substrate that supports the Raman enhancement.[61] To further confirm this point, a simple simulation was performed. In this simulation, the Pt−CO and Ru−CO stretching bands for atop CO were calculated by using the Lorentz equation and taking the peak values as 490.7 and 497.4 cm^{-1}, respectively. These values are the average of independent measurements on three samples (Figure 3). The calculated Pt−CO and Ru−CO stretching bands were then added together to simulate the measured spectra. The resultant spectra showed a single peak, and its position depends on the intensity of the two bands. To fit experimentally obtained ν_{M-CO}, an adjustable parameter was multiplied to the Ru−CO band intensity to reflect its weaker intensity as compared to the Pt−CO band on a given PtRu surface. The best fit was obtained when this parameter is 0.4, and the calculated points are included in Figure 3 as open circles. A 2.5 times intensity decrease on Ru is reasonable,[62] given that the Ru islands are probably two to three atomic layer thin patches.[48,59,63] These results strongly suggest that the addition of Ru to the Pt surface does not change the Pt−CO bond significantly. In harmony with this, the CO binding energy, evaluated from the temperature programmed desorption spectra, lowers by only 2 kcal/mol with the addition of 0.25 ML Ru to Pt(110).[10,64] The insignificant change of the Pt−CO stretching frequency observed in the present work is contrary to the DFT calculation results, which predict a more than 50 cm^{-1} red-shift in ν_{Pt-CO} when the Ru coverage is 50%.[23] The SERS study presented here represents the first in situ direct probing of ν_{Pt-CO} on Ru-modified Pt. The absence of a significant change in ν_{Pt-CO} suggests that the ligand effect, if present, may only affect Pt sites within two to three atomic distances from Ru islands, and the effect is weak.

SERS during Methanol Oxidation. One advantage of SERS as compared to surface infrared spectroscopy is its high surface sensitivity coming from the surface enhancement effect. This allows for real-time studies that can provide detailed molecular level insights into the reaction mechanism, as demonstrated by Weaver and co-workers.[65−67] This strategy entails recording the SER spectrum concurrently with the cyclic voltammogram and relating the spectral transitions to the faradaic current changes. Exploiting the same tactic, we recorded SER spectra simultaneously with cyclic voltammograms for methanol oxidation on Pt and Ru-modified Pt. Displayed in Figure 4 are results from two representative examples of such studies, obtained on a 2 ML Pt film (Figure 4A) and a Ru-modified 2 ML Pt with $\theta_{Ru} = 0.6$ (Figure 4B) in 0.1 M $HClO_4$ and 1 M MeOH. The applied potential was swept concomitantly at 1 mV/s from −0.2 to +0.8 V and returned. The corresponding cyclic voltammograms are shown in Figure 1B. The spectral acquisition time was 20 s; therefore, each spectrum encompasses 20 mV. The spectrograph

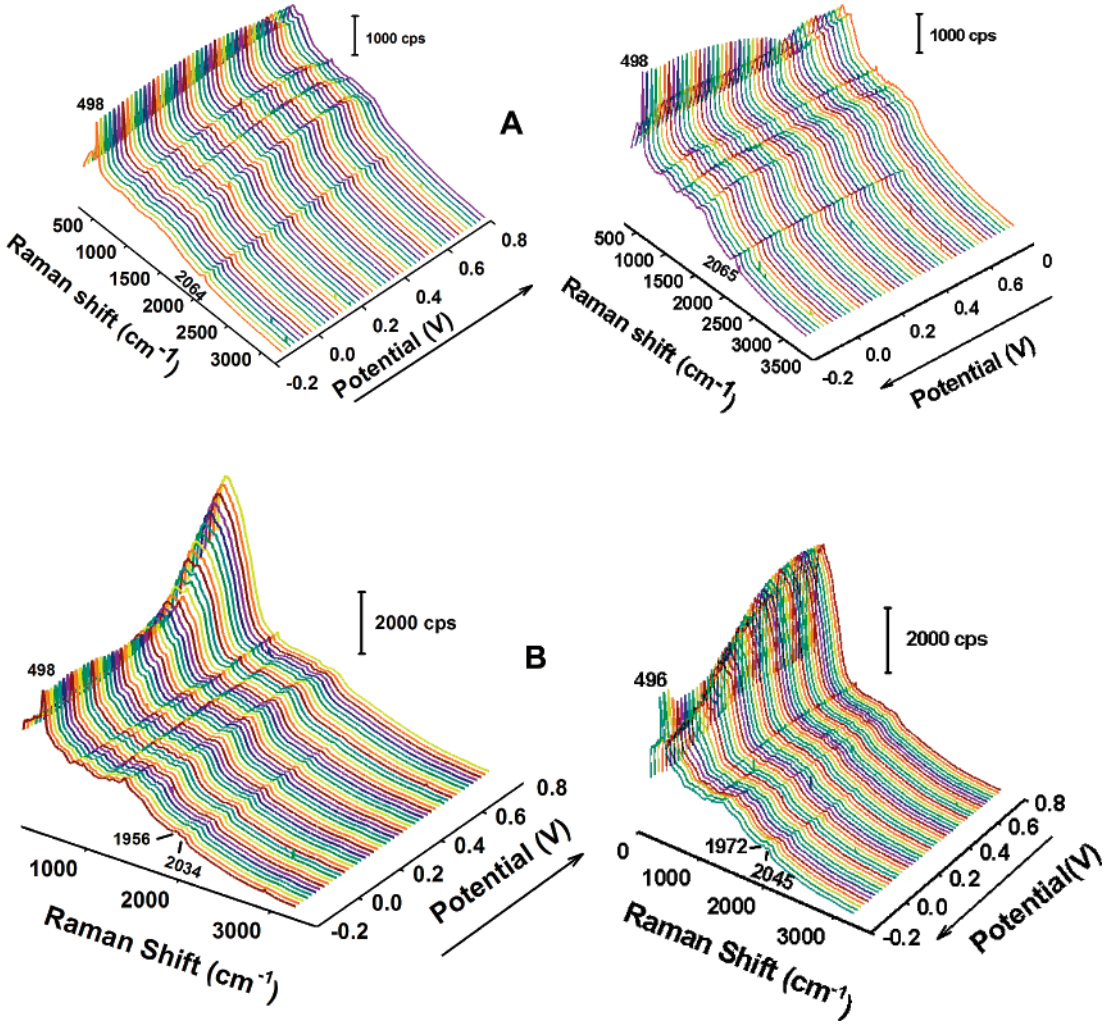

Figure 4. SER spectra obtained on 2 ML Pt (A) and 2 ML Pt/Ru-0.6 (B) in 1 M methanol + 0.1 M $HClO_4$ simultaneously with the cyclic voltammograms shown in Figure 1B. Applied potential scan rate: 1 mV s^{-1}. Acquisition time for each spectrum: 20 s. Spectrograph grating: 300 g/mm.

grating was 300 groove/mm, rendering a spectrum covering 300−3000 cm^{-1} with a resolution of 8 cm^{-1}.

The spectra show significant potential-dependent changes in both the lower frequency and the C−O stretching regions. To demonstrate these changes clearly, spectra at selective potentials are replotted in Figures 5 and 6, with the emphasis on the C−O stretching region and the lower frequency region where the M−CO and metal oxide bands are located in the C−O stretching region. The spectra were stacked sequentially from bottom to top, with the initial spectrum at the bottom. The electrode potential alongside each spectrum is referred to as the average of the values at the beginning and end of the acquisition of that spectrum.

On 2 ML Pt, the electrode was exposed to methanol at −0.2 V. Methanol oxidation to form adsorbed CO already occurred at this potential as was evident by the appearance of Pt−CO and corresponding C−O stretching bands. The two bands at 412 and 496 cm^{-1} in the lower frequency region (Figure 5A) can be assigned to the Pt−CO stretching from bridging and atop CO, respectively, and the 2060 cm^{-1} band at the higher frequency region (Figure 5B) is from the C−O stretching of atop CO. The corresponding ν_{CO} of bridging CO is also present but much weaker (Figure 5B). The observed red-shift in ν_{CO} frequency as compared to that obtained from CO adsorbed on Pt from the CO-saturated solution is in agreement with a number of previous studies using IRAS and is due to the lower CO

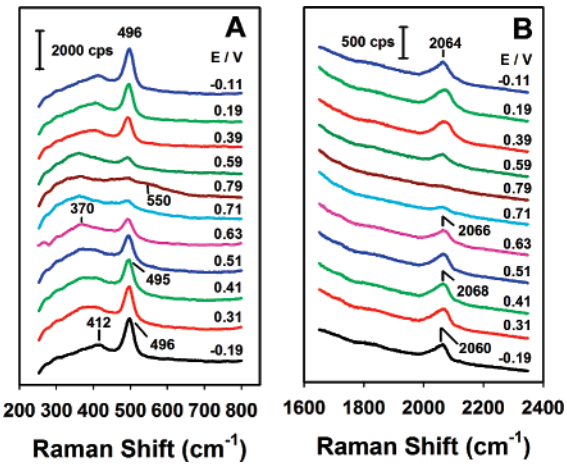

Figure 5. Selected members of SER spectra on 2 ML Pt in 1 M MeOH + 0.1 M $HClO_4$ from Figure 4A. The applied potential is indicated alongside each spectrum.

coverage.[13,14] Sweeping the potential up to 0.4 V, the spectra in both frequency regions are largely the same, except for the blue-shift of ν_{CO} and the red-shift of ν_{Pt-CO} expected from the electrochemical Stark tuning effect.[60] When the potential reached above 0.4 V, a significant spectral transition occurred. The intensity of ν_{CO} and ν_{Pt-CO} decreased. In the lower frequency region, an additional band located at around 370 cm^{-1} emerged.

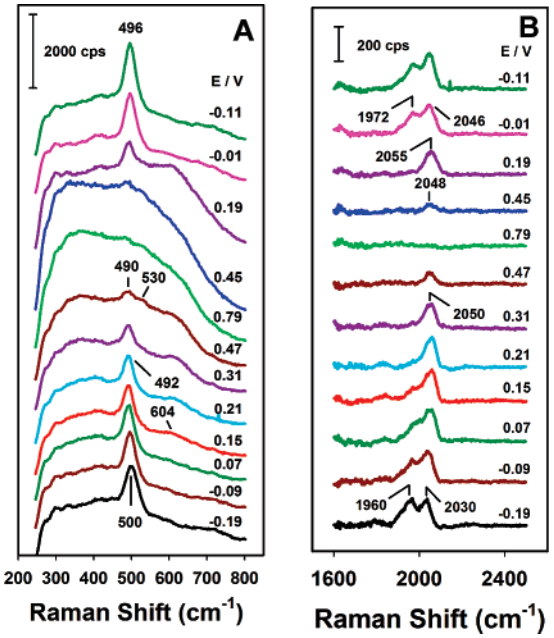

Figure 6. Selected SER spectra from Figure 4B obtained on 2 ML Pt/Ru-0.6 in 1 M methanol + 0.1 M $HClO_4$. The electrode potential is indicated alongside the corresponding spectrum.

This band is likely from the Pt oxide.[67,68] Further scanning the potential to 0.63 V, the C−O stretching band intensity kept decreasing, and the 370 cm^{-1} band became stronger. The ν_{CO} band eventually diminished at around 0.8 V, and at the lower frequency region, two broad bands at 370 and 550 cm^{-1} were dominant. By comparing this to the SER spectra obtained without methanol, these two bands can be assigned to Pt oxides.[67,68] Upon returning the potential to more negative values, ν_{CO} regained intensity starting at about 0.7 V (spectrum not shown), as did ν_{Pt-CO}. The 550 cm^{-1} oxide band disappeared at this potential as well. The intensity of ν_{CO} and ν_{Pt-CO} remained unchanged after the potential was returned to below 0.45 V, and the oxide band at 370 cm^{-1} was not discernible.

These potential-dependent spectral transitions when combined with the concurrently recorded cyclic volatammogram provide insights into the methanol oxidation on Pt. In the potential region between −0.2 and +0.4 V, although the methanol oxidation can occur as evident from the formation of CO_{ads} at −0.2 V, it is poisoned by the CO_{ads}. Once the oxidation of adsorbed CO begins at around 0.4 V, which is signified by the decrease of CO band intensity and also consistent with the CO stripping voltammogram (Figure 1A, dotted trace), methanol oxidation takes off as shown by the increasing current in the cyclic volatammogram (Figure 1B, dotted trace). From the SER spectra, it is evident that surface oxidation occurs at about 0.5 V. In the potential range of 0.4−0.63 V, the kinetic gain of methanol oxidation from the higher overpotential overcomes the loss of active Pt sites due to the formation of Pt surface oxides, which are inactive for methanol oxidation. Above 0.63 V, however, the loss of active sites becomes dominant and eventually shuts off the reaction. The appearance of a methanol oxidation current peak at 0.63 V is a result of the balance between the decrease of the activity due to the surface oxidation and the increase of the reaction driving force by the applied potential. The current peak did not result from the methanol diffusion as a similar peak potential was observed in the rotating disk voltammogram (Figure S2A). In the reversed potential scan, the surface oxide reduction regenerates the surface-active sites for methanol oxidation below ca. 0.7 V. The accumulation of CO on the surface, signified by the increase of the ν_{CO} and ν_{Pt-CO} band intensities, blocks the reaction at lower potentials.

We now turn to Ru-modified Pt. The applied potential was initially held at −0.4 V for 3 min to ensure complete reduction of ruthenium oxides. Then, the potential was switched to −0.2 V, and a measured amount of pure methanol was added to make up a 1 M solution. The SER spectrum displays two C−O stretching bands at −0.2 V in the higher frequency region (Figure 6B). The one centered at around 2030 cm^{-1} can be attributed to the linear adsorbed CO on the Pt sites and the other one at 1960 cm^{-1} is from CO adsorbed on the Ru sites.[15,56,69] Interestingly, in a separate experiment, the two ν_{CO} bands were also observed at −0.4 V, albeit at slightly lower frequencies, indicating that methanol oxidation to form adsorbed CO already occurred at this potential. However, this was not observed on pure Pt film. With the potential increased to −0.1 V, the ν_{CO} intensity from Ru sites decreased by more than 10%, and the ν_{CO} from Pt sites increased by more than 20%. Meanwhile, the center frequency of both bands increased. Further increasing the potential up to 0.2 V, the ν_{CO} from the Ru sites gradually lost its intensity and finally disappeared at 0.2 V. The ν_{CO} intensity from the Pt sites remained unchanged, and its frequency increased to 2058 cm^{-1}. In this potential range, the ν_{CO} from bridging CO on Pt sites was clearly discernible at 1820−1830 cm^{-1}. From 0.2 to 0.6 V, the ν_{CO} band intensity decreased gradually and completely diminished at ca. 0.6 V. With the potential returns from 0.8 V, the ν_{CO} band from CO on Pt sites reappeared at around 0.5 V, and its intensity kept increasing. Upon returning the potential to 0.15 V, the ν_{CO} from CO adsorption on Ru sites re-emerged. The intensity of the two ν_{CO} bands from Pt and Ru sites kept growing until −0.1 V. The potential-dependent SER spectra in the ν_{CO} region are largely in agreement with the in situ FTIR results obtained on CO adsorption on Ru-modified Pt(111)[59] and Pt nanoparticles,[15] as well as methanol oxidation on Ru-modified Pt(111) and PtRu alloys.[56,69] The appearance of a ν_{CO} band from CO on Ru sites suggests the formation of sizable Ru islands,[15,21] which explains that the optimal Ru content for methanol oxidation observed here is higher than that expected from well-mixed PtRu alloys (vide supra).[70] The formation of nanometer scale Ru islands on Ru-modified Pt(111) has been confirmed by in situ STM studies.[56,57]

Of essential importance here are the potential-dependent SER spectra at the lower frequency region. At ca. −0.2 V, a sharp peak appears at 500 cm^{-1}, which can be assigned to the M−CO stretch from CO adsorbed on both Pt and Ru sites. The ν_{Pt-CO} and ν_{Ru-CO} values cannot be distinguished because the grating used in this case (300 groove/mm) does not provide enough resolution, and the two bands are broad (cf. Figure 2). As the potential was swept to more positive values, the ν_{M-CO} band shifted to smaller values and reached 492 cm^{-1} at ca. 0.05 V. This red-shift is much larger than the typical 15 cm^{-1}/V Stark tuning slope,[60] suggesting that other factors contribute to this shift, most likely the increasing CO coverage, as is evident in the ν_{CO} band intensity. Further increasing the potential to 0.15 V, a new broad band appeared at about 604 cm^{-1}, which can be assigned to the Ru oxides.[71−73] At this potential, the M−CO stretching band intensity also decreased slightly, consistent with the oxidation of CO on the Ru sites. When the potential reached 0.3 V, the M−CO band intensity decreased significantly, signifying the oxidation of CO. With the potential excursed to more positive values, the M−CO band diminished, and the broad Ru oxide band at 604 cm^{-1} intensified. Meanwhile, an additional band at around 530 cm^{-1} emerged. This band was

also observed on Ru-coated Au in 0.1 M $HClO_4$,[41] and together with the 604 cm^{-1} band has been attributed to RuO_2.[41,74] Similar Ru oxide bands were also observed at the same potentials on Ru-modified Pt in 0.1 M $HClO_4$ without methanol. At potentials above 0.5 V, the spectrum became very broad as a result of overlapping oxide bands from both Ru and Pt oxidation.[68,75] It is interesting to note that a band at ca. 300 cm^{-1} was observed on Ru-coated Au in 0.1 M $HClO_4$ either with or without methanol.[41,68] This band is, however, absent on the PtRu surface (Figure 6A) and sometimes even on Ru-coated Au.[75] The assignment of this band is still unclear. It can be from either the Ru−O bending mode or the Raman inactive RuO_2 lattice vibration.[41,68] The 370 cm^{-1} band observed on the Pt surface (Figure 5A) is very weak on the PtRu surface due probably to the high coverage of Ru. On the reversed potential scan, the M−CO band reappeared at about 0.45 V, while the Ru oxide bands were still present. With the potential scanned to more negative values, the M−CO band intensified. When the potential reached about 0 V, the M−CO band intensity was stable, and the Ru oxide bands were no longer discernible, suggesting the removal of the Ru oxides from the surface. O'Grady and co-workers studied the structure of Pt/Ru catalysts using X-ray absorption near edge structure (XANES).[30] They found that metal oxides were reduced to the metallic form when the PtRu catalysts were placed in an electrochemical cell and held at 0.1 V versus RHE.

When these potential-dependent spectral transitions are considered together with the concomitantly recorded cyclic voltammograms, significant new insights can be obtained for methanol oxidation on Ru-modified Pt. In the cyclic voltammograms, the methanol oxidation peak current appears at around 0.45 V, which is significantly more negative than that on pure Pt. The appearance of the current peak is again not due to the methanol diffusion, as indicated by the similar peak potential observed in the quiescent (Figure 1B) and rotating disk electrode (Figure S2B) voltammograms. In the Raman spectrum, it is clearly evident that a significant amount of Ru is oxidized at this potential, suggesting that the Ru oxidation prevents further methanol oxidation. Note that at this potential, the Pt surface oxidation is insignificant (cf. Figure 5). The inhibition of methanol oxidation by Ru oxides is further confirmed in the reversed potential scan. Although on a pure Pt surface, the methanol oxidation current increases sharply after the potential returns to below 0.7 V and reached nearly the same peak value as in the positive scan, on Ru-modified Pt, the methanol oxidation current is much smaller (cf. Figure 1B). From the Raman spectra, the Ru sites are still in the oxide form until the potential moves to below 0 V. These observations indicate that the presence of Ru oxides inhibits methanol oxidation on the Pt sites, even when the Pt sites are in the metallic form. This conclusion is in line with that obtained by Kim et al. in an XPS study of Ru-modified Pt(111) electrodes.[29] Further support for this conclusion can be found in separate cyclic voltammetry studies of methanol oxidation on Ru-modified Pt(111)[57] and SERS studies of Ru oxidation−reduction.[68] Note that the current is normalized to the available Pt sites in Figure 1B. The fact that the current is much smaller than that on the positive scan suggests that the inhibition is an electronic effect.

Our findings are consistent with various in situ X-ray absorption studies on the carbon-supported PtRu catalysts, which confirm the importance of the metallic Ru.[30−32] However, the inhibition effect of the Ru oxides on the methanol oxidation is in contrast to the conclusions reached by Rolison and co-workers.[25,26] Their ex situ XPS studies suggest that bulk hydrous Ru oxide is the preferred component in the PtRu catalysts. As pointed out by O'Grady et al.,[30] this disparity emphasizes the importance of in situ studies. Although the chemical nature of Ru oxide(s) inhibiting methanol oxidation remains to be uncovered, the agreement between the results from our Ru-modified Pt thin films and those from the practical PtRu catalysts suggests that the information provided by the present study is generally applicable. It would be interesting to further examine the practically used PtRu catalyst and other systems by using the tactics employed here. Efforts in this direction are underway in our laboratory.

Conclusion

In summary, we have shown that in situ surface-enhanced Raman spectroscopy is a powerful tool for studying catalytically important interfaces. When combined with electrochemical techniques, new insights can be obtained to advance our understanding of the effects of the reaction promoters, such as Ru. It is found that the addition of Ru to Pt does not weaken the Pt−CO bond. On both Pt and Ru-modified Pt surface, the methanol oxidation is inhibited by the formation of surface oxides. For the Ru-modified Pt surfaces, the formation of Ru oxides is detrimental to the methanol oxidation. The agreement of the present SERS results with the findings from in situ surface infrared and X-ray absorption studies assures that the information provided by SERS is representative of the entire surface, instead of special sites. Most importantly, SERS is able to yield insights that are not straightforwardly attainable by other spectroscopic methods, as shown in this study. The information provided by SERS, when combined with that from other techniques, gives us a more complete understanding of methanol oxidation on PtRu catalysts. We therefore have reason to be optimistic that SERS will play an increasingly important role in the field of fuel cell electrocatalysis.

Acknowledgment. This work was partially supported by Research Corporation (RI1218) and by Miami University through a CFR grant.

Supporting Information Available: Cyclic voltammograms of Ru-coated Au and PtRu-0.6 in 0.1 M $HClO_4$, and RDE voltammograms of methanol oxidation on Pt and PtRu-0.45 in 1 M methanol + 0.1 M $HClO_4$. This material is available free of charge via the Internet at http://pubs.acs.org.

References and Notes

(1) Parsons, R.; VanderNoot, T. *J. Electroanal. Chem.* **1988**, *257*, 9−45.
(2) Hamnett, A. In *Interfacial Electrochemistry: Theory, Experiment, and Applications*; Wieckowski, A., Ed.; Marcel Dekker: New York, 1999; p 843.
(3) Ross, P. N. In *Electrocatalysis*; Lipkowski, J., Ross, P. N., Eds.; Wiley-VCH: New York, 1998; Vol. 3, pp 43−74.
(4) Lamy, C.; Leger, J.-M.; Srinivasan, S. In *Modern Aspects of Electrochemistry*; Bockris, J. O. M., White, R. E., Conway, B. E., Eds.; Kluwer Academic/Plenum: New York, 2001; Vol. 34, p 53.
(5) Watanabe, M.; Motoo, S. *J. Electroanal. Chem.* **1975**, *60*, 267−273.
(6) Krausa, M.; Vielstich, W. *J. Electroanal. Chem.* **1994**, *379*, 307−314.
(7) Buatier de Mongeot, F.; Scherer, M.; Gleich, B.; Kopatzki, E.; Behm, R. J. *Surf. Sci.* **1998**, *411*, 249−262.
(8) Frelink, T.; Visscher, W.; Van Veen, J. A. R. *Langmuir* **1996**, *12*, 3702−3708.
(9) Tong, Y.; Kim, H. S.; Babu, P. K.; Waszczuk, P.; Wieckowski, A.; Oldfield, E. *J. Am. Chem. Soc.* **2002**, *124*, 468−473.
(10) Lu, C.; Rice, C.; Masel, R. I.; Babu, P. K.; Waszczuk, P.; Kim, H. S.; Oldfield, E.; Wieckowski, A. *J. Phys. Chem. B* **2002**, *106*, 9581−9589.
(11) McBreen, J.; Mukerjee, S. *J. Electrochem. Soc.* **1995**, *142*, 3399−3404.

(12) Korzeniewski, C.; Basnayake, R.; Vijayaraghavan, G.; Li, Z. R.; Xu, S. H.; Casadonte, D. J. *Surf. Sci.* **2004**, *573*, 100−108.
(13) Park, S.; Tong, Y. T.; Wieckowski, A.; Weaver, M. J. *Langmuir* **2002**, *18*, 3233−3240.
(14) Park, S.; Wasileski, S. A.; Weaver, M. J. *J. Phys. Chem. B* **2001**, *105*, 9719−9725.
(15) Park, S.; Wieckowski, A.; Weaver, M. J. *J. Am. Chem. Soc.* **2003**, *125*, 2282−2290.
(16) Iwasita, T. In *Handbook of Fuel Cells*; Vielstich, W., Gasteiger, H. A., Lamm, A., Eds.; John Wiley and Sons: New York, 2003; Vol. 2, pp 603−624.
(17) Lu, G. Q.; Lagutchev, A.; Dlott, D. D.; Wieckowski, A. *Surf. Sci.* **2005**, *585*, 3−16.
(18) Lu, G. Q.; White, J. O.; Wieckowski, A. *Surf. Sci.* **2004**, *564*, 131−140.
(19) Korzeniewski, C. *Crit. Rev. Anal. Chem.* **1997**, *27*, 81−102.
(20) Iwasita, T.; Nart, F. C.; Vielstich, W. *Ber. Bunsen-Ges. Phys. Chem.* **1990**, *94*, 1030−1034.
(21) Zou, S.; Villegas, I.; Stuhlmann, C.; Weaver, M. J. *Electrochim. Acta* **1998**, *43*, 2811−2824.
(22) Koper, M. T. M.; Shubina, T. E.; van Santen, R. A. *J. Phys. Chem. B* **2002**, *106*, 686−692.
(23) Liao, M. S.; Cabrera, C. R.; Ishikawa, Y. *Surf. Sci.* **2000**, *445*, 267−282.
(24) Gurau, B.; Viswanathan, R.; Liu, R. X.; Lafrenz, T. J.; Ley, K. L.; Smotkin, E. S.; Reddington, E.; Sapienza, A.; Chan, B. C.; Mallouk, T. E.; Sarangapani, S. *J. Phys. Chem. B* **1998**, *102*, 9997−10003.
(25) Rolison, D. R.; Hagans, P. L.; Swider, K. E.; Long, J. W. *Langmuir* **1999**, *15*, 774−779.
(26) Long, J. W.; Stroud, R. M.; Swider-Lyons, K. E.; Rolison, D. R. *J. Phys. Chem. B* **2000**, *104*, 9772−9776.
(27) Kennedy, B. J.; Smith, A. W. *J. Electroanal. Chem.* **1990**, *293*, 103−110.
(28) Lasch, K.; Jorissen, L.; Friedrich, K. A.; Garche, J. *J. Solid State Electrochem.* **2003**, *7*, 619−625.
(29) Kim, H.; de Moraes, I. R.; Tremiliosi, G.; Haasch, R.; Wieckowski, A. *Surf. Sci.* **2001**, *474*, 203−212.
(30) O'Grady, W. E.; Hagans, P. L.; Pandya, K. I.; Maricle, D. L. *Langmuir* **2001**, *17*, 3047−3050.
(31) Russell, A. E.; Maniguet, S.; Mathew, R. J.; Yao, J.; Roberts, M. A.; Thompsett, D. *J. Power Sources* **2001**, *96*, 226−232.
(32) Viswanathan, R.; Hou, G. Y.; Liu, R. X.; Bare, S. R.; Modica, F.; Mickelson, G.; Segre, C. U.; Leyarovska, N.; Smotkin, E. S. *J. Phys. Chem. B* **2002**, *106*, 3458−3465.
(33) Pettinger, B. In *Adsorption of Molecules at Metal Electrodes*; Lipkowski, J., Ross, P. N., Eds.; VCH: New York, 1992; p 285.
(34) Tian, Z. Q.; Ren, B. *Annu. Rev. Phys. Chem.* **2004**, *55*, 197−229.
(35) Weaver, M. J.; Zou, S.; Chan, H. Y. *Anal. Chem.* **2000**, *72*, 38−47.
(36) Mrozek, M. F.; Xie, Y.; Weaver, M. J. *Anal. Chem.* **2001**, *73*, 5953−5960.
(37) Zou, S.; Weaver, M. J. *Anal. Chem.* **1998**, *70*, 2387−2395.
(38) Tian, Z. Q.; Ren, B.; Wu, D. Y. *J. Phys. Chem. B* **2002**, *106*, 9463−9483.
(39) Cai, W. B.; Ren, B.; Li, X. Q.; She, C. X.; Liu, F. M.; Cai, X. W.; Tian, Z. Q. *Surf. Sci.* **1998**, *406*, 9−22.
(40) She, C. X.; Xiang, J.; Ren, B.; Wang, X. C.; Zhong, Q. L.; Tian, Z. Q. *J. Korean Electrochem. Soc.* **2002**, *5*, 221−225.
(41) Yang, H.; Yang, Y.; Zou, S. *J. Phys. Chem. B* **2006**, *110*, 17296−17301.
(42) Gao, P.; Gosztola, D.; Leung, L. W. H.; Weaver, M. J. *J. Electroanal. Chem.* **1987**, *233*, 211−222.
(43) Brankovic, S. R.; Wang, J. X.; Adzic, R. R. *Surf. Sci.* **2001**, *474*, 173−179.
(44) Chrzanowski, W.; Wieckowski, A. *Langmuir* **1997**, *13*, 5974−5978.
(45) Wilke, T.; Gao, X.; Takoudis, C. G.; Weaver, M. J. *Langmuir* **1991**, *7*, 714−721.
(46) Gruenbaum, S. M.; Henney, M. H.; Kumar, S.; Zou, S. Z. *J. Phys. Chem. B* **2006**, *110*, 4782−4792.
(47) Jaiswal, A.; Tavakoli, K. G.; Zou, S. Z. *Anal. Chem.* **2006**, *78*, 120−124.
(48) Lin, W. F.; Zei, M. S.; Eiswirth, M.; Ertl, G.; Iwasita, T.; Vielstich, W. *J. Phys. Chem. B* **1999**, *103*, 6968−6977.
(49) Davies, J. C.; Hayden, B. E.; Pegg, D. J. *Surf. Sci.* **2000**, *467*, 118−130.
(50) Waszczuk, P.; Lu, G. Q.; Wieckowski, A.; Lu, C.; Rice, C.; Masel, R. I. *Electrochim. Acta* **2002**, *47*, 3637−3652.
(51) Kabbabi, A.; Faure, R.; Durand, R.; Beden, B.; Hahn, F.; Leger, J. M.; Lamy, C. *J. Electroanal. Chem.* **1998**, *444*, 41−53.
(52) Maillard, F.; Gloaguen, F.; Leger, J. M. *J. Appl. Electrochem.* **2003**, *33*, 1−8.
(53) Gasteiger, H. A.; Markovic, N.; Ross, P. N.; Cairns, E. J. *J. Phys. Chem.* **1994**, *98*, 617−625.
(54) Maillard, F.; Eikerling, M.; Cherstiouk, O. V.; Schreier, S.; Savinova, E.; Stimming, U. *Faraday Discuss.* **2004**, *125*, 357−377.
(55) Waszczuk, P.; Solla-Gullon, J.; Kim, H. S.; Tong, Y. Y.; Montiel, V.; Aldaz, A.; Wieckowski, A. *J. Catal.* **2001**, *203*, 1−6.
(56) Iwasita, T.; Hoster, H.; John-Anacker, A.; Lin, W. F.; Vielstich, W. *Langmuir* **2000**, *16*, 522−529.
(57) Crown, A.; Moraes, I. R.; Wieckowski, A. *J. Electroanal. Chem.* **2001**, *500*, 333−343.
(58) Park, S.; Yang, P.; Corredor, P.; Weaver, M. J. **2002**, *124*, 2428−2429.
(59) Friedrich, K. A.; Geyzers, K. P.; Dickinson, A. J.; Stimming, U. *J. Electroanal. Chem.* **2002**, *524*, 261−272.
(60) Zou, S. Z.; Weaver, M. J. *J. Phys. Chem.* **1996**, *100*, 4237−4242.
(61) Zou, S.; Weaver, M. J.; Li, X. Q.; Ren, B.; Tian, Z. Q. *J. Phys. Chem. B* **1999**, *103*, 4218−4222.
(62) Wasileski, S. A.; Zou, S. Z.; Weaver, M. J. *Appl. Spectrosc.* **2000**, *54*, 761−772.
(63) Herrero, E.; Feliu, J. M.; Wieckowski, A. *Langmuir* **1999**, *15*, 4944−4948.
(64) Lu, C.; Masel, R. I. *J. Phys. Chem. B* **2001**, *105*, 9793−9797.
(65) Gao, P.; Gosztola, D.; Weaver, M. J. *J. Phys. Chem.* **1988**, *92*, 7122−7130.
(66) Gao, P.; Gosztola, D.; Weaver, M. J. *J. Phys. Chem.* **1989**, *93*, 3753−3760.
(67) Zhang, Y.; Weaver, M. J. *J. Electroanal. Chem.* **1993**, *354*, 173−188.
(68) Zhang, Y.; Gao, X.; Weaver, M. J. *J. Phys. Chem.* **1993**, *97*, 8656−8663.
(69) Batista, E. A.; Hoster, H.; Iwasita, T. *J. Electroanal. Chem.* **2003**, *554*−*555*, 265−271.
(70) Gasteiger, H. A.; Markovic, N.; Ross, P. N.; Cairns, E. J. *J. Phys. Chem.* **1993**, *97*, 12020−12029.
(71) Chan, H. Y. H.; Takoudis, C. C.; Weaver, M. J. *J. Catal.* **1997**, *172*, 336−345.
(72) Thomas, G. E.; Weinberg, W. H. *J. Chem. Phys.* **1979**, *70*, 954−961.
(73) Xie, J.; Mitchell, W. J.; Lyons, K. J.; Wang, Y. Q.; Weinberg, W. H. *J. Vac. Sci. Technol., A* **1994**, *12*, 2210−2214.
(74) Mar, S. Y.; Chen, C. S.; Huang, Y. S.; Tiong, K. K. *Appl. Surf. Sci.* **1995**, *90*, 497−504.
(75) Chan, H. Y. H.; Zou, S. Z.; Weaver, M. J. *J. Phys. Chem. B* **1999**, *103*, 11141−11151.